ADVANCED MATERIALS INTERFACES
Open Access
www.advmatinterfaces.de

MoS_2 Synthesized by Atomic Layer Deposition as Cu Diffusion Barrier

*Johanna (Sanne) H. Deijkers, Arthur A. de Jong, Miika J. Mattinen, Jeff J. P. M. Schulpen, Marcel A. Verheijen, Hessel Sprey, Jan Willem Maes, Wilhelmus (Erwin) M. M. Kessels, Ageeth A. Bol, and Adriaan J. M. Mackus**

Miniaturization in integrated circuits requires that the Cu diffusion barriers located in interconnects between the Cu metal line and the dielectric material should scale down. Replacing the conventional TaN with a 2D transition metal dichalcogenide barrier potentially offers the opportunity to scale to 1–2 nm thick barriers. In this article, it is demonstrated that MoS_2 synthesized by atomic layer deposition (ALD) can be employed as a Cu diffusion barrier. ALD offers a controlled growth process at back-end-of-line (BEOL) compatible temperatures. MoS_2 films of different thicknesses (i.e., 2.2, 4.3, and 6.5 nm) are tested by time-dependent dielectric breakdown (TDDB) measurements, demonstrating that ALD-grown MoS_2 can enhance dielectric lifetime by a factor up to 17 at an electric field of 7 MV cm^{-1}. Extrapolation to lower E-fields shows that the MoS_2 barriers prepared by ALD have at least an order of magnitude higher median-time-to-failure during device operation at 0.5 MV cm^{-1} compared with MoS_2 barriers prepared by other methods. By scaling the thickness further down in future work, the ALD MoS_2 films can be applied as ultrathin Cu diffusion barriers.

1. Introduction

For many years, there is a trend in miniaturization of electronics with transistors becoming smaller and faster. The interconnect structure linking the transistors, schematically shown in **Figure 1**A, has to be reduced in size as well.[1] Therefore, metal lines, consisting of Cu and a liner/diffusion barrier, are required to shrink. By scaling the barrier, there will be a relatively larger volume available for the Cu such that the resistivity remains low. However, thin barriers fail as illustrated in Figure 1C. The conventional barrier material TaN[2–6] can be scaled down to a thickness of only 3 nm until it starts to fail.[7–9] Therefore, there is an interest in new barrier materials, such as two-dimensional (2D) materials that could potentially work as diffusion barrier at smaller thicknesses[9–15] (Figure 1C).

2D materials, such as graphene and h-BN, have strong covalent bonds in the in-plane direction and weak van der Waals bonds between the planes. 2D transition metal dichalcogenides (2D-TMDs) are a class of 2D materials with the chemical formula of MX_2, with M a transition metal atom and X a chalcogen atom, forming an atomically thin layer.[16,17] Various 2D materials, such as graphene, h-BN, (Nb-doped) MoS_2, and TaS_x, have been investigated experimentally for Cu blocking, and these materials can work as a diffusion barrier down to only a (few) monolayer(s) in thickness.[10–15] The main hypothesis in those studies is that the Cu diffusion in a 2D material takes place from grain boundary to grain boundary, adding lateral diffusion in between adjacent 2D layers to the total diffusion path, as schematically shown in Figure 1B. Consistent with this mechanism, graphene barriers of two and three layers exhibit an improvement in median-time-to-failure of a factor two and three at the device-operating electric field of 0.5 MV cm^{-1}, respectively, compared with single-layer graphene.[11] Structures with a chemical vapor deposition (CVD) grown MoS_2 barrier compared with barrierless structures display an improvement of three orders of magnitude at 0.5 MV cm^{-1}.[12] The longest time-to-breakdown of $>1.25 \times 10^4$ s at 7 MV cm^{-1} has been reported for 2.8 nm MoS_2 doped with 3% Nb.[14] In those previous studies, the diffusion barrier layers have been manufactured either by a transfer process,[10–12] by

J. (S) H. Deijkers, A. A. de Jong, M. J. Mattinen, J. J. P. M. Schulpen, M. A. Verheijen, W. (E) M. M. Kessels, A. A. Bol, A. J. M. Mackus
Department of Applied Physics and Science Education
Eindhoven University of Technology
Eindhoven 5600 MB, The Netherlands
E-mail: a.j.m.mackus@tue.nl

M. A. Verheijen
Eurofins Materials Science BV
High Tech Campus
Eindhoven 5656 AE, The Netherlands

H. Sprey, J. W. Maes
ASM Belgium
Leuven B3001, Belgium

A. A. Bol
Department of Chemistry
University of Michigan
Ann Arbor, MI 48109, USA

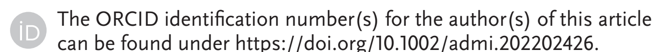
The ORCID identification number(s) for the author(s) of this article can be found under https://doi.org/10.1002/admi.202202426.

© 2023 The Authors. Advanced Materials Interfaces published by Wiley-VCH GmbH. This is an open access article under the terms of the Creative Commons Attribution License, which permits use, distribution and reproduction in any medium, provided the original work is properly cited.

DOI: 10.1002/admi.202202426

 © 2023 The Authors. Advanced Materials Interfaces published by Wiley-VCH GmbH

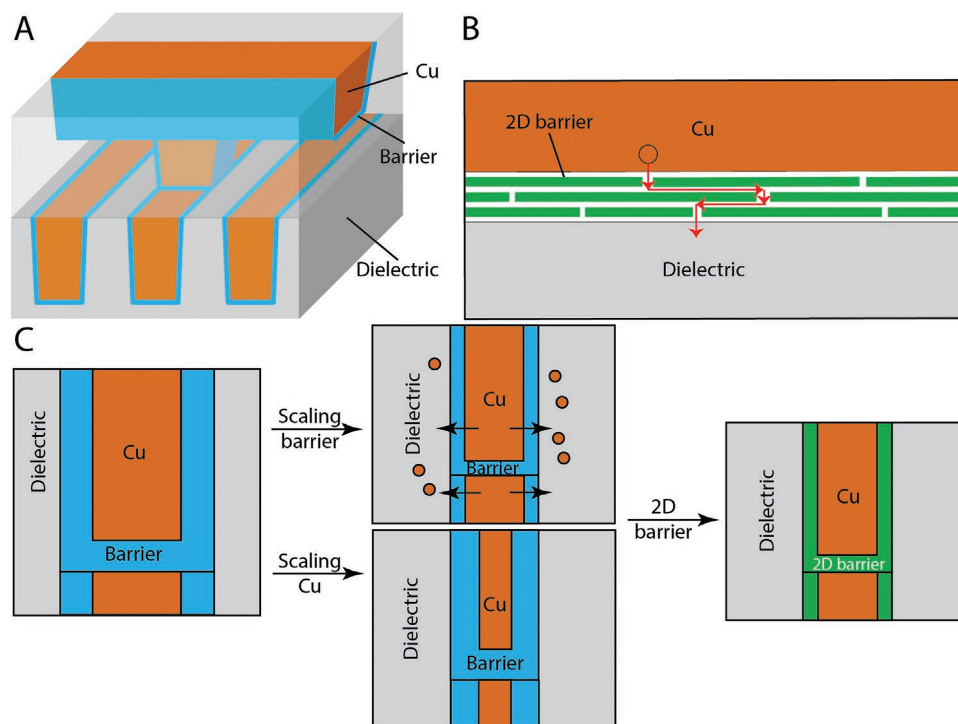

Figure 1. A) Schematic illustration of an interconnect structure with metal lines and a via. B) Cu diffusion mechanism path through a 2D barrier proposed by Li et al.,[11] indicated by the red arrows, via grain boundaries, with additional lateral diffusion. The 2D barrier consists of multiple single sheet grains where consecutive 2D layers do not have joint grain boundaries. C) Effect of interconnect scaling on the Cu volume in the metal line/via with a scaled or constant barrier thickness. Cu diffusion takes place if the barrier is too thin. Replacing the barrier by a thin 2D film could result in sufficient Cu blocking and limited reduction of the Cu volume.

direct deposition using CVD[12–14] or by plasma sulfurization of the corresponding metal.[15] Transfer processes are not scalable and high temperature ($T > 500$ °C) processes, such as CVD, are not back-end-of-line (BEOL) compatible.

Another method for the synthesis of 2D-TMDs is atomic layer deposition (ALD).[18] In an ALD cycle, the precursor provides the transition metal atom, and subsequently the coreactant (e.g., H_2S gas or plasma) sulfurizes the adsorbed transition metal precursor. This happens by self-limiting reactions of the precursor molecules and coreactant species with the available surface chemical groups.[19] The morphology and properties of the 2D film can be tuned for the desired application by adjusting the process conditions, such as the temperature and pressure.[20–24] 2D-TMD films grown by ALD are not necessarily similar to 2D-TMD films grown by other methods, e.g., the grain size and uniformity can differ.[18] ALD has several benefits for 2D-TMD synthesis, i.e., it offers: (i) processes at BEOL-compatible temperatures; (ii) conformal growth as a result of the self-limiting half-reactions, as is required for demanding 3D structures; (iii) optimal thickness control; and (iv) control over the film morphology. These merits make ALD an interesting alternative to the transfer and CVD processes, especially for barrier synthesis.

In this work, ALD was used to deposit MoS_2 as diffusion barrier for interconnect technology at 450 °C. The MoS_2 films serve as a demonstrator for ALD 2D-TMD-based Cu diffusion barriers and are tested on planar capacitor structures, following the example of other demonstrator studies. Using extensive time-dependent dielectric breakdown (TDDB) measurements, we show that ALD MoS_2 films efficiently block Cu diffusion for different barrier thicknesses and electric fields. It is shown that the ALD-grown MoS_2 films have great potential as barrier layers in device applications as they meet the "10 years" industry standard at $E \leq 0.5$ MV cm^{-1}.

2. Results and Discussions

MoS_2 deposited by ALD consists of small, ≈10 nm, crystalline grains,[20,25,26] visible in the top-view high-angle annular dark field scanning transmission electron microscopy (HAADF STEM) images of **Figure** 2A–E. The thickness of each film was measured by atomic force microscopy, see the Supporting Information. The Raman spectra confirming the crystallinity and the semiconducting 2H phase of MoS_2 (resistivity ≈10^9 µΩ cm) can be found in the Supporting Information as well. The growth of ALD MoS_2 initially starts with horizontal layers on the substrate and predominantly occurs at the reactive edges of grains.[20] Vertical structures (fins) can form when two laterally growing grains encounter each other.[23] Such vertical fins are visible in the STEM images in Figure 2A–E as white lines representing vertical sheets of MoS_2. The films are relatively rough due to the presence of fins. The 6.5-nm thick MoS_2 films have, on average, more fins than the 4.3-nm MoS_2 thick films as further quantified in the Supporting Information. The fins likely affect the diffusion path of Cu through the MoS_2

 © 2023 The Authors. Advanced Materials Interfaces published by Wiley-VCH GmbH

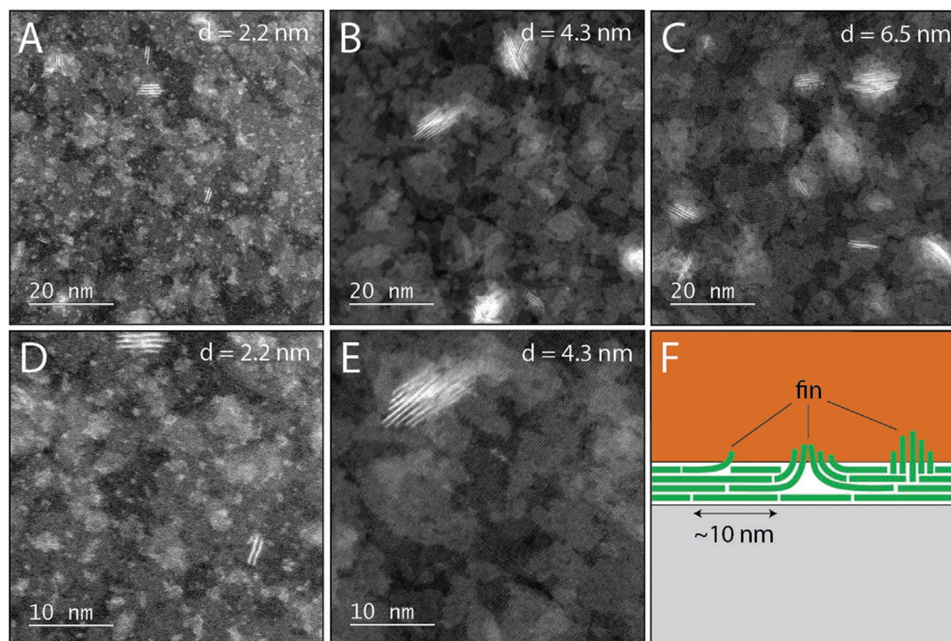

Figure 2. HAADF top-view STEM images at: A–C) 2.5 million times magnification and D,E) 5 million times magnification of different thicknesses of ALD MoS_2: (A,D) 2.2 nm, (B,E) 4.3 nm, and (C) 6.5 nm MoS_2. Some contamination of the sample is visible on the 2.2 nm MoS_2 images (A,D) in the form of white dots. F) Schematic cross-sectional representation of the MoS_2 film showing different types of fin structures.

barrier. As shown in Figure 1B, the diffusion of Cu is expected to take place from vertical grain boundary to vertical grain boundary, due to the high-energy barrier for diffusion through the basal plane of MoS_2.[9] Consequently, there is additional lateral (horizontal) diffusion in between the basal planes. The diffusion along the grain boundaries is assumed to be faster than the lateral diffusion under the influence of a perpendicular electric field. Fin structures, as schematically shown in Figure 2F, likely add an extra vertical diffusion path.

In order to function as a Cu diffusion barrier, the MoS_2 must form a closed film and thus fully cover the dielectric underneath. The 5 million times magnification HAADF STEM image of the 2.2-nm MoS_2 film in Figure 2D shows that on the entire surface there is MoS_2 deposition, indicated by the presence of Mo atoms in the entire image. In the atomic-resolution HAADF STEM image, the heavier Mo atoms are visible as bright dots, while the S atoms cannot be visualized. The pattern of the Mo atoms shows the crystal structure as expected from MoS_2. There are some small black spots visible on the surface, but these are assumed to be point defects in the crystal. Diffusion of Cu through point defects is not likely due to a relatively high-energy barrier.[27] The islands with discrete levels in gray scale in Figure 2B,C,E reflect the various numbers of 2D layers.

TDDB measurements were conducted at multiple electric field strengths to investigate the influence of the electric field on the barrier performance. The resulting time-to-breakdown (t_{BD}) is represented in the cumulative distribution plots shown in **Figure 3**A–D for every thickness. Different positions on a 3×3 cm^2 sample were measured and no correlation between the time-to-breakdown and position was observed. Moreover, multiple samples were deposited during one run and there was no correlation between the t_{BD} and location in the reactor chamber, confirming the uniformity of deposition that is expected from ALD. The plots reveal a longer median-time-to-failure ($TTF_{50\%}$), i.e., an improved device performance, as compared with barrierless structures for all electric field strengths and thicknesses of MoS_2. At 7 MV cm^{-1}, $TTF_{50\%}$ increases with a factor 2.6, 5.8, and 17 for 2.2, 4.3, and 6.5 nm MoS_2, respectively. As a reference, transferred h-BN and single-layer MoS_2 grown by low-temperature CVD show an improvement of a factor 4.6 and 2.1 at the same E-field.[12,13]

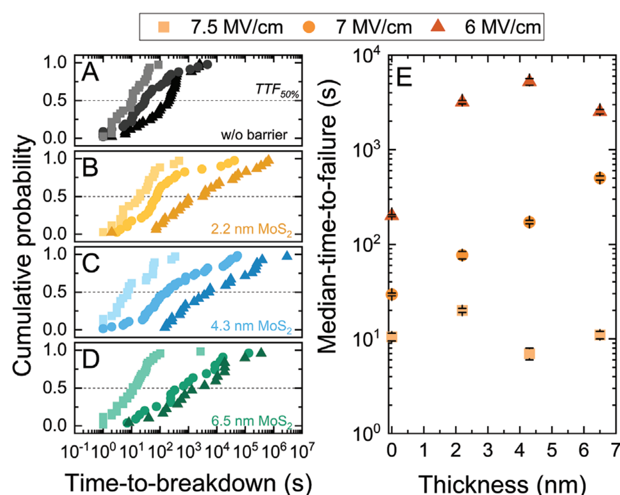

Figure 3. Cumulative distribution of time-to-breakdown of structures: A) without a barrier and B–D) with different thicknesses of MoS_2 barriers under various electric field stresses. The median-time-to-failure ($TTF_{50\%}$) is indicated with the dashed line. E) Median-time-to-failure as a function of the MoS_2 barrier thickness.

© 2023 The Authors. Advanced Materials Interfaces published by Wiley-VCH GmbH

The trend of $TTF_{50\%}$ with MoS_2 thickness is shown in Figure 3E, which is different for each electric field. Structures with a 2.2 nm MoS_2 film show a factor 2–15 improvement as compared with the barrierless reference structures at all three electric fields. The structures with a 4.3 or 6.5 nm MoS_2 film show substantial improvement of $TTF_{50\%}$ at 6 and 7 MV cm^{-1}. From the different graphs in Figure 3, it can be concluded that the 4.3 and 6.5 nm thick MoS_2 films are more strongly affected by the incrementing E-field than the 2.2 nm thick film. The difference between the barrier performance of the three thicknesses can likely be explained by the morphology of the MoS_2 films. Thicker films have more horizontal 2D layers, and thus effectively a longer diffusion path, enhancing the barrier performance. However, from a thickness of 4 nm, there are more fins for increasingly thick films, resulting in a trade-off between the different diffusion contributions. At higher E-fields, the influence of the diffusion through the fins most likely becomes stronger, since the E-field is in the same (vertical) direction as the fins. Thus, the $TTF_{50\%}$ of thicker films is affected more by an increasing E-field than the $TTF_{50\%}$ of relatively thin films.

The electric fields used in the TDDB measurements are higher than the electric fields in an actual device. The median-time-to-failure can be extrapolated to lower E-fields using the conservative E-model[28] in order to obtain insight into long-term operation in devices. The extrapolation of the ALD-grown MoS_2 results of this work, presented in **Figure 4**, shows that all three thicknesses meet the "10 years" industry standard at $E \leq 0.5$ MV cm^{-1}. TDDB results of MoS_2 films from the literature[12,13] are shown in Figure 4 together with our ALD MoS_2 results, in order to compare different synthesis processes for MoS_2 barriers. A comparison including h-BN[12] and TaS_x[15] barriers can be found in the Supporting Information. The $TTF_{50\%}$ values of the ALD MoS_2 films are in general better compared with the other MoS_2 films. The extrapolation to low E-fields of the ALD MoS_2 shows a higher slope and thus a better barrier performance at low E-fields. Although the ALD MoS_2 films are thicker than the other MoS_2 films, the $TTF_{50\%}$ of 2.2 nm MoS_2 extrapolated to 0.5 MV cm^{-1} is more than an order of magnitude higher compared with the $TTF_{50\%}$ of the 1.3 nm CVD MoS_2, which shows the best extrapolation of the literature results.[12]

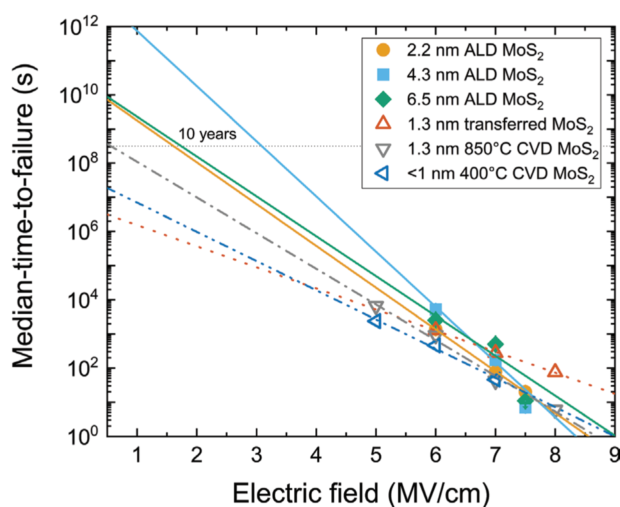

Figure 4. Extrapolation of the median-time-to-failure data to low electric fields, shown by the linear fit according to the E-model.[28] The horizontal dashed line indicates a time of 10 years. ALD MoS_2 results are from this work. Transferred MoS_2 and 850 °C CVD MoS_2 results are from Lo et al. (2017)[12] and 400 °C CVD MoS_2 results are from Lo et al. (2018).[13]

3. Conclusions

In this work, we demonstrate that MoS_2 synthesized by ALD at a BEOL-compatible temperature can serve as a Cu diffusion barrier. The barrier performance was assessed using TDDB measurements at different electric fields. The morphology resulting from the ALD growth affects the barrier performance for thick (>4 nm) films. The thinnest films in this work (2.2 nm) were least influenced by the electric field, which is promising for further thickness downscaling. ALD MoS_2 layers outperform CVD-synthesized MoS_2, especially at lower E-fields. Future work will focus on thickness scaling and investigating other 2D-TMDs as a Cu diffusion barrier. The results highlight the potential of ALD for 2D-TMD barriers in the BEOL.

4. Experimental Section

A plasma-enhanced ALD (PE-ALD) process as developed by Sharma et al.[20] was used to deposit different thicknesses of MoS_2 at a set table temperature of 450 °C. PE-ALD processes are attractive for nanoscale device fabrication, due to the high reactivity of the plasma.[29] The substrate temperature was ≈350 °C due to limited thermal contact between the substrate and the table.[30] The depositions were executed using an Oxford Instruments FlexAL reactor equipped with a remote inductively coupled plasma source. As precursor, $Mo(N^tBu)_2(NMe_2)_2$ (98%, Sigma-Aldrich) was employed. The precursor was contained in a stainless-steel canister, which was heated to 50 °C. A 50 sccm Ar bubbling flow was applied to facilitate precursor delivery into the reaction chamber. After each precursor dose (6 s) and plasma coreactant exposure (20 s), an intermediate purge step (10 s) with 100 sccm of Ar flow was implemented. A plasma mixture of 8 sccm H_2S, 2 sccm H_2, and 40 sccm Ar was used as the coreactant. The plasma was operated at a power of 100 W at a pressure of ≈6 mTorr. At the used table temperature of 450 °C, the precursor dose showed soft-saturating behavior.[20] It could not be excluded that this soft-saturation was resulting from precursor decomposition. However, due to the short precursor dose (6 s), it was expected that precursor decomposition had little to no contribution to the growth or to the barrier performance. The deposited films consisted of stoichiometric MoS_2 with a Mo:S ratio of 1:2.0.[31]

Capacitor structures, illustrated in the inset of **Figure 5**, consisting of p++ Si base with 90 nm dry thermal SiO_2 as the dielectric and with a Cu/Al electrode on the top and an Al electrode on the bottom, were used for TDDB measurements. The top electrodes were deposited through a shadow mask, where the first 5 nm of Cu was deposited either with e-beam evaporation or soft-impact sputtering, for which no difference in performance was observed in the investigations. Subsequently, the remaining 25 nm Cu and the Al were sputtered at regular conditions. Likewise, the bottom Al electrode was sputtered at regular conditions over the whole area. The adhesion between the MoS_2 and the electrode, tested by a Scotch tape test, was better than the adhesion between the MoS_2 and SiO_2, see the Supporting Information. TDDB measurements were performed at room temperature by applying a constant electric field across the capacitor structure. During the measurement, the current was measured as a function of time, and the t_{BD} was determined from the sharp increase

© 2023 The Authors. Advanced Materials Interfaces published by Wiley-VCH GmbH

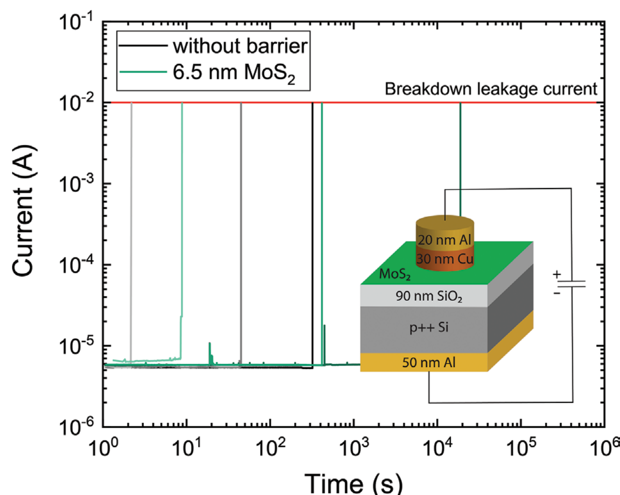

Figure 5. (I, t)-graphs of several individual TDDB measurements of samples without a barrier layer and with a 6.5 nm MoS_2 barrier layer, measured at 6 MV cm^{-1}. The red line indicates the breakdown leakage current threshold. The inset shows a schematic representation of capacitor structures used for TDDB measurements.

in current where the leakage current exceeded 1.3×10^{-2} µA µm^{-2},[12] as shown in Figure 5.

Single time-to-breakdown values did not provide information on the barrier performance, since dielectric breakdown is a stochastic process. Therefore, the t_{BD} of at least 15 structures was recorded for each barrier thickness. Each t_{BD} was assigned a probability according to the cumulative probability of failure formula presented by Fothergill.[32] The standard deviation of the median was determined by the statistical spread on a logarithmic scale.

As a reference, 10 nm node chips have a minimum metal pitch of 36 nm and $V = 0.70$ V, resulting in a field of $E = 0.39$ MV cm^{-1}.[33] As time-to-failure studies using realistic electric fields are extremely time-consuming, accelerated tests was performed where a series of higher electric fields were used. The $TTF_{50\%}$ is the time for which 50% of the samples had shown breakdown. The $TTF_{50\%}$ values resulting from the TDDB measurements at 6, 7, and 7.5 MV cm^{-1} could be extrapolated to lower E-fields as shown in Figure 4. This extrapolation provided insight in the performance at operating fields of $E \leq 0.5$ MV cm^{-1} ($E = 0.39$ MV cm^{-1} for reference 10 nm node chips) without requiring extremely long measurement times. The E-model ($\ln(TTF_{50\%}) \approx -\gamma E$) was the most conservative model to extrapolate $TTF_{50\%}$ to lower E-fields[28] and was used here to not overestimate the barrier performance.

Supporting Information

Supporting Information is available from the Wiley Online Library or from the author.

Acknowledgements

This work was performed with the support of ASM International. The authors thank C.O. van Bommel, J.J.L.M. Meulendijks, J.J.A. Zeebregts, A.B. Schrader, P. Sanders, and B. Krishnamoorthy for technical assistance and the Physics of Nanostructures (FNA) research group for supplying resources to deposit electrodes for the TDDB measurements. Solliance and the Dutch province of Noord-Brabant are acknowledged for funding the TEM facility.

Conflict of Interest

The authors declare no conflict of interest.

Data Availability Statement

The data that support the findings of this study are available from the corresponding author upon reasonable request.

Keywords

atomic layer deposition, back-end-of-line, Cu diffusion barrier, MoS_2, time-dependent dielectric breakdown

Received: December 1, 2022
Revised: January 31, 2023
Published online: March 27, 2023

[1] M. R. Baklanov, C. Adelmann, L. Zhao, S. De Gendt, *ECS J. Solid State Sci. Technol.* **2015**, *4*, Y1.
[2] K.-H. Min, *J. Vac. Sci. Technol. B Microelectron. Nanom. Struct.* **1996**, *14*, 3263.
[3] R. Hübner, M. Hecker, N. Mattern, V. Hoffmann, K. Wetzig, C. Wenger, H. J. Engelmann, C. Wenzel, E. Zschech, J. W. Bartha, *Thin Solid Films* **2003**, *437*, 248.
[4] H. Kizil, C. Steinbrüchel, *Thin Solid Films* **2004**, *449*, 158.
[5] H. C. M. Knoops, L. Baggetto, E. Langereis, M. C. M. van de Sanden, J. H. Klootwijk, F. Roozeboom, R. A. H. Niessen, P. H. L. Notten, W. M. M. Kessels, *J. Electrochem. Soc.* **2008**, *155*, G287.
[6] O. van der Straten, X. Zhang, K. Motoyama, C. Penny, J. Maniscalco, S. Knupp, *ECS Meet. Abstr.* **2014**, *MA2014-02*, 1611.
[7] Z. Wu, R. Li, X. Xie, W. Suen, J. Tseng, N. Bekiaris, R. Vinnakota, K. Kashefizadeh, M. Naik, *2018 IEEE Int. Interconnect Technol. Conf.* **2018**, *149*, 2018.
[8] C. Witt, K. B. Yeap, A. Lesniewska, D. Wan, N. Jordan, I. Ciofi, C. Wu, Z. Tokei, *2018 IEEE Int. Interconnect Technol. Conf.* **2018**, *54*, 2018.
[9] C. L. Lo, B. A. Helfrecht, Y. He, D. M. Guzman, N. Onofrio, S. Zhang, D. Weinstein, A. Strachan, Z. Chen, *J. Appl. Phys.* **2020**, *128*, 080903.
[10] B. S. Nguyen, J. F. Lin, D. C. Perng, *Appl. Phys. Lett.* **2014**, *104*, 082105.
[11] L. Li, X. Chen, C. H. Wang, J. Cao, S. Lee, A. Tang, C. Ahn, S. Singha Roy, M. S. Arnold, H. S. P. Wong, *ACS Nano* **2015**, *9*, 8361.
[12] C. L. Lo, M. Catalano, K. K. H. Smithe, L. Wang, S. Zhang, E. Pop, M. J. Kim, Z. Chen, *npj 2D Mater. Appl.* **2017**, *1*, 42.
[13] C. L. Lo, K. Zhang, R. S. Smith, K. Shah, J. A. Robinson, Z. Chen, *IEEE Electron Device Lett.* **2018**, *39*, 873.
[14] R. Zhao, C. L. Lo, F. Zhang, R. K. Ghosh, T. Knobloch, M. Terrones, Z. Chen, J. Robinson, *Adv. Mater. Interfaces* **2019**, *6*, 1901055.
[15] C. L. Lo, M. Catalano, A. Khosravi, W. Ge, Y. Ji, D. Y. Zemlyanov, L. Wang, R. Addou, Y. Liu, R. M. Wallace, M. J. Kim, Z. Chen, *Adv. Mater.* **2019**, *31*, 1902397.
[16] M. Samadi, N. Sarikhani, M. Zirak, H. Zhang, H. L. Zhang, A. Z. Moshfegh, *Nanoscale Horiz.* **2018**, *3*, 90.
[17] S. Manzeli, D. Ovchinnikov, D. Pasquier, O. V. Yazyev, A. Kis, *Nat. Rev. Mater.* **2017**, *2*, 17033.
[18] M. Mattinen, M. Leskelä, M. Ritala, *Adv. Mater. Interfaces* **2021**, *8*, 2001677.

 © 2023 The Authors. Advanced Materials Interfaces published by Wiley-VCH GmbH

[19] H. C. M. Knoops, S. E. Potts, A. A. Bol, W. M. M. Kessels, *Atomic Layer Deposition*, 2nd ed., Elsevier B. V., Boston **2015**, https://doi.org/10.1016/B978-0-444-63304-0.00027-5.
[20] A. Sharma, M. A. Verheijen, L. Wu, S. Karwal, V. Vandalon, H. C. M. Knoops, R. S. Sundaram, J. P. Hofmann, W. M. M. Kessels, A. A. Bol, *Nanoscale* **2018**, *10*, 8615.
[21] S. Balasubramanyam, M. Shirazi, M. A. Bloodgood, L. Wu, M. A. Verheijen, V. Vandalon, W. M. M. Kessels, J. P. Hofmann, A. A. Bol, *Chem. Mater.* **2019**, *31*, 5104.
[22] S. B. Basuvalingam, Y. Zhang, M. A. Bloodgood, R. H. Godiksen, A. G. Curto, J. P. Hofmann, M. A. Verheijen, W. M. M. Kessels, A. A. Bol, *Chem. Mater.* **2019**, *31*, 9354.
[23] S. Balasubramanyam, M. A. Bloodgood, M. Van Ommeren, T. Faraz, V. Vandalon, W. M. M. Kessels, M. A. Verheijen, A. A. Bol, *ACS Appl. Mater. Interfaces* **2020**, *12*, 3873.
[24] J. J. P. M. Schulpen, M. A. Verheijen, W. M. M. (Erwin) Kessels, V. Vandalon, A. A. Bol, *2D Mater.* **2022**, *9*, 025016.
[25] A. Sharma, R. Mahlouji, L. Wu, M. A. Verheijen, V. Vandalon, S. Balasubramanyam, J. P. Hofmann, W. M. M. Erwin Kessels, A. A. Bol, *Nanotechnology* **2020**, *31*, 255603.
[26] R. Mahlouji, M. A. Verheijen, Y. Zhang, J. P. Hofmann, W. M. M. Kessels, A. A. Bol, *Adv. Electron. Mater.* **2022**, *8*, 2100781.
[27] Y. Zhao, Z. Liu, T. Sun, L. Zhang, W. Jie, X. Wang, Y. Xie, Y. H. Tsang, H. Long, Y. Chai, *ACS Nano* **2014**, *8*, 12601.
[28] G. S. Haase, E. T. Ogawa, J. W. McPherson, *J. Appl. Phys.* **2005**, *98*, 034503.
[29] H. Kim, I. K. Oh, *Jpn. J. Appl. Phys.* **2014**, *53*, 03DA01.
[30] H. C. M. Knoops, E. M. J. Braeken, K. De Peuter, S. E. Potts, S. Haukka, V. Pore, W. M. M. Kessels, *ACS Appl. Mater. Interfaces* **2015**, *7*, 19857.
[31] M. Mattinen, F. Gity, E. Coleman, J. F. A. Vonk, M. A. Verheijen, R. Duffy, W. M. M. Kessels, A. A. Bol, *Chem. Mater.* **2022**, *34*, 7280.
[32] J. C. Fothergill, *IEEE Trans. Electr. Insul.* **1990**, *25*, 489.
[33] C. Auth, A. Aliyarukunju, M. Asoro, D. Bergstrom, V. Bhagwat, J. Birdsall, N. Bisnik, M. Buehler, V. Chikarmane, G. Ding, Q. Fu, H. Gomez, W. Han, D. Hanken, M. Haran, M. Hattendorf, R. Heussner, H. Hiramatsu, B. Ho, S. Joloviar, I. Jin, S. Joshi, S. Kirby, S. Kosaraju, H. Kothari, G. Leatherman, K. Lee, J. Leib, A. Madhavan, K. Marla, et al., in *2017 IEEE International Electron Devices Meeting (IEDM)*, **2017**, 29.1.1-29.1.4, https://doi.org/10.1109/IEDM.2017.8268472.

© 2023 The Authors. Advanced Materials Interfaces published by Wiley-VCH GmbH